Nanoscale

RSC Publishing

COMMUNICATION

View Article Online
View Journal | View Issue

Fabrication of (001)-oriented monoclinic WO_3 films on FTO substrates†

Cite this: *Nanoscale*, 2013, **5**, 5279

Jin You Zheng,‡ Guang Song,‡ Chang Woo Kim and Young Soo Kang*

Received 24th February 2013
Accepted 14th April 2013

DOI: 10.1039/c3nr00964e

www.rsc.org/nanoscale

(001)-oriented monoclinic nanorod and microplate WO_3 films are fabricated on commercial FTO-coated glass substrates by a rubbing seed layer and a spin-coating seed layer assisted by hydrothermal reactions. The nanorod film obtained by the rubbing seed layer assisted by hydrothermal reactions is more regular and perpendicular to the substrate.

Tungsten trioxide (WO_3), an n-type semiconductor with a smaller band gap of *ca.* 2.8 eV than that of TiO_2 ($E_g = 3.2$ eV), is one of the most well-known photocatalysts for water splitting under visible light irradiation.[1] The hole mobility and diffusion length of WO_3 are 10 $cm^2\ V^{-1}\ s^{-1}$ and 0.15 μm, respectively, much better than those of α-Fe_2O_3 (10^{-2} to 10^{-1} $cm^2\ V^{-1}\ s^{-1}$ and 2–20 nm).[2] In addition, WO_3 possesses high resistance against photocorrosion and good chemical stability in an acidic environment (pH < 4) under solar illumination. Depending on the temperature and pressure, the bulk WO_3 crystal phase can be classified into five forms:[3,4] tetragonal (α-WO_3), orthorhombic (β-WO_3), monoclinic I (γ-WO_3), triclinic (δ-WO_3) and monoclinic II (ε-WO_3). The monoclinic I (γ-WO_3) is the most stable phase in bulk WO_3 at room temperature, which can be described as a distorted $2 \times 2 \times 2$ superstructure of the normal cubic ReO_3-type unit cell, by tilting the WO_6 octahedra and displacing the central W atom.[4] In the crystal structure of γ-monoclinic WO_3, the bond lengths are nearly symmetric along the [100] direction, but long–short alternating along both [010] and [001] directions.[5]

The photocatalytic reactivity of a semiconductor photocatalyst is affected by its electronic and surface atomic structures, which sensitively depend on the crystal facet with different orientations. Li *et al.* reported that the (001) surface of γ-monoclinic WO_3 has the lowest surface energy compared with other facets.[6] Recently, Valdés and Kroes showed that the photooxidation of water on the γ-monoclinic WO_3 (200) surface requires an overpotential of 1.04 V, 1.10 V for the (020) surface and 1.05 V for the (002) surface by using DFT calculations.[7] Jin *et al.*[8] have performed DFT calculations on the structural and electronic properties of the (001) facet of γ-monoclinic WO_3. Most recently, Xie *et al.*[9] reported a quasi-cubic-like monoclinic WO_3 crystal with a nearly equal percentage of {002}, {200} and {020} facets, which show a much higher photocatalytic oxidation activity of H_2O for O_2 evolution; a {002} dominant rectangular sheet-like WO_3 with an elevated conduction band minimum of 0.3 eV can reduce CO_2 to CH_4 under light illumination. In addition, they also gave a surface energy order of {002} (1.56 J m^{-2}) > {020} (1.54 J m^{-2}) > {200} (1.43 J m^{-2}), which indicates that {200} is the most stable and {002} is the most unstable. The active sites at the catalyst surface and the underlying reaction mechanisms in photocatalytic processes of WO_3 are still not clear and are attracting many researchers' interest.

Considering the practical application, WO_3 thin films are more popular than powder types since film types can be used for electrochromic devices,[10–12] gas sensors[13,14] and photochemical electrodes.[15,16] WO_3 films can be prepared by various methods such as sputtering,[17–19] evaporation,[18] chemical vapor deposition (CVD),[20] pulsed laser deposition (PLD),[21] molecular beam epitaxy (MBE),[22] sol–gel,[23] electrochemical deposition,[16] hydrothermal reaction[10–12,15,24] and so on. However, the properties of the films are significantly affected by the films' crystallinity and texture which are dependent on various process parameters and the type of substrate used.[19] In addition, as mentioned above, since the properties of WO_3 crystals sensitively depend on the dominant crystal facets, it is important to achieve the epitaxial growth of WO_3 films. Many studies on the investigation of the epitaxial growth of WO_3 films on sapphire,[17–20] MgO[17] and $SrTiO_3$ (ref. 19) substrates by sputtering or CVD methods have been reported. However, these fabrication techniques are

Korea Center for Artificial Photosynthesis (KCAP), Department of Chemistry, Sogang University, Seoul 121-742, South Korea. E-mail: yskang@sogang.ac.kr; Fax: +82-2-701-0967

† Electronic supplementary information (ESI) available: Experimental details and characterization (Fig. S1–S4). See DOI: 10.1039/c3nr00964e

‡ These authors contributed equally to the work.

expensive and require extreme experimental conditions such as high temperature and high vacuum; in addition, these substrates are electrical insulators although their crystal lattices highly match with WO_3. For using in solar conversion devices such as solar cells and solar water splitting, it is very important to achieve the epitaxial growth of WO_3 films on transparent conductive substrates such as indium-doped tin oxide (ITO) and fluorine-doped tin oxide (FTO) coated glasses. The comparison between ITO and FTO is that the electrical resistance of ITO will be increased tremendously while the resistance of FTO is stable at high temperature annealing.[25]

Particularly, Sun's[10–12,15] and Grimes's[24] groups have performed many studies on fabrication of WO_3 films on FTO coated glass by a hydrothermal method; however, these films are not one facet oriented. It is challenging and promising to produce (001) facet oriented monoclinic tungsten trioxide films. Herein, (001)-oriented monoclinic nanorod and microplate WO_3 films are fabricated on commercial FTO substrates by a rubbing seed layer (RSL) or spin-coating seed layer (SSL) assisted by hydrothermal reactions using different capping agents. The photocurrents of nanorod and microplate films are comparatively discussed.

Fig. 1 shows the SEM images and XRD patterns of seed layers made by spin-coating and rubbing methods after calcination treatment. The reflection peaks of the produced WO_3 films completely fit with monoclinic phase WO_3 (JCPDS no. 43-1035). The differences between these two methods are as follows: (i) the sizes of WO_3 seeds on FTO are different. The seeds made by the spin-coating method are very small (<50 nm) and the layer composed of them is attached to FTO very well. In contrast, the size of WO_3 seeds made by the rubbing method is about 300 nm, which is completely dependent on the size of the rubbing crystals as shown in Fig. S1(a).† The size limitation for direct attachment is from about 0.5 μm to 3 μm with respect to rate, degree of close packing, uniform orientation of the assembled microcrystals, substrate area, and ecological considerations.[26] Therefore, compared to the other accurate technologies such as PLD, MBE and so on, the rubbing method is not good at making ultra thin monolayer films using the particles with the thickness lower than 200 nm. However, the rubbing method can fabricate films with one-axis orientation without necessarily considering the crystal lattice matching between rubbing materials and substrates. Herein, the rubbing layer is not perfect since the assembled WO_3 nanoplates are not uniform enough and the size of which is around 300 nm, less than the lower limit size of 500 nm. (ii) The crystallinity and dominant crystal facet of WO_3 seed layers are different. The spin-coating seed layer has low crystallinity and the dominant crystal facet cannot be controlled artificially as shown in Fig. 1(c)c1. For the rubbing seed layer, the crystallinity is very high and the dominant crystal facet is (002), which can be attributed to the intrinsic nature of a single crystalline WO_3 nanoplate with dominant facet (002). Some other crystal facets are also rarely exposed, such as (020) and (200). The peak intensity ratios of (002) to (020) and (200) are $I_{(002)}/I_{(020)} = 6.08$ and $I_{(002)}/I_{(200)} = 6.88$ as shown in Table 1. Compared with those of WO_3 powder samples for rubbing, the ratios of dominant crystal facet (002) to (020) and (200) increase about 5 times as shown in Table 1. Therefore, we believe that if the homogeneous micro-sized single crystalline WO_3 plates can be made, only the (002)-oriented WO_3 film can be prepared on substrates such as glass, FTO or ITO coated glass by the rubbing method.

Fig. 2(a) and (b) show the top-view and cross-sectional SEM images of the WO_3 film obtained by RSL assisted by a hydrothermal method using citric acid as a capping agent. The vertically oriented WO_3 nanorod array film with a thickness of *ca.* 900 nm was obtained and the transverses of nanorods were square or rectangle. It indicated that WO_3 nanorods grew along the [001] orientation. With the same natural conclusion, the WO_3 crystal would preferably grow along the [001] orientation because the (001) facet is more active than the other facets.[27] The XRD pattern in Fig. 2(c) also completely fits with monoclinic phase tungsten trioxide (JCPDS no. 43-1035). The $I_{(002)}/I_{(020)}$ is 16.73 and the $I_{(002)}/I_{(200)}$ is 25.73. They are much higher than $I_{(002)}/I_{(020)}$ and $I_{(002)}/I_{(200)}$ of WO_3 powder and the rubbing seed layer. The (002) facets in all nanorod crystals obtained by RSL assisted by hydrothermal reactions are the most exposed facets under X-ray irradiation. To study the photoelectrochemical property of this film,

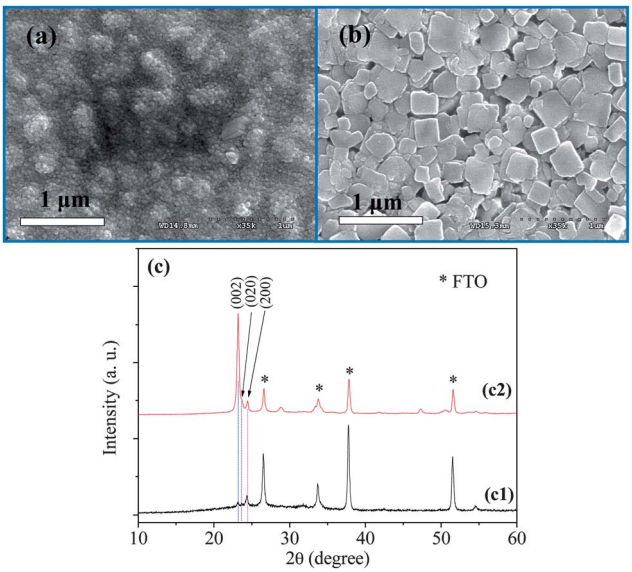

Fig. 1 SEM images and XRD patterns of the seed layers made by (a and c1) spin-coating and (b and c2) rubbing methods after calcination in air at 500 °C for 2 h.

Table 1 XRD peak intensity ratios of (002) to (020) and (200) of different samples. RSL: rubbing seed layer; SSL: spin-coating seed layer

Samples		$I_{(002)}/I_{(020)}$	$I_{(002)}/I_{(200)}$
WO_3 powder (see Fig. S1)		1.33	1.27
RSL		6.08	6.88
RSL after hydrothermal growth		16.73	25.73
SSL		1.17	0.71
SSL after hydrothermal growth[a]		9.60	5.38
SSL assisted by the hydrothermal method at different pHs	pH 1.9	1.86	4.25
	pH 2.3	0.83	1.58
	pH 2.5	2.21	3.05

[a] The crystal phase mixed with a little orthorhombic $WO_3 \cdot 0.33H_2O$.

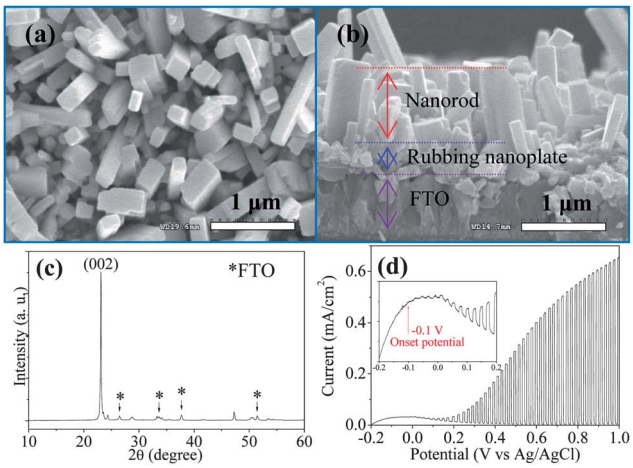

Fig. 2 (a) Top-view and (b) cross-sectional SEM images and (c) XRD pattern of the as-synthesized WO_3 film by the rubbing seed layer assisted by a hydrothermal method at 180 °C for 24 h using 0.1 mol citric acid as a capping agent. (d) Photocurrent of the film after calcination in air at 500 °C for 2 h. The inset is a magnified curve from −0.2 to 0.2 V.

the current–potential property was checked in 0.5 M Na_2SO_4 solution (pH 6.3) under chopped (1 Hz: light on and off) 1 sun light illumination. The photocurrent onset potential is approximately −0.1 V *vs.* Ag/AgCl and the photocurrent is *ca.* 0.65 mA cm^{-2} at 1.0 V *vs.* Ag/AgCl.

Considering that the WO_3 product is sensitive to the pH of reaction solution, the morphology study of the resultant product dependent on the pH of solution was carried out at different pHs of the reaction solution as shown in Fig. 3. Herein, we used SSL assisted by a hydrothermal method since the RSL was not perfectly uniform as mentioned previously. All of the rod arrays obtained at different pHs were not completely vertical. At initial pH 1.9, the cuboid rods were very sharp and had very clear surfaces. However, some incomplete plate-like particles existed in the film. As the pH was increased to 2.3, the cuboid nanorods became homogeneous; the most transverses of nanorods were square. When pH was 2.5, the surfaces of rods became rough and were not perfectly cuboid any more. One possible reason is that the surface of WO_3 can be dissolved at relatively high pH in the hydrothermal reaction. Another reason is that the pH affected the concentration of the real functional group – carboxyl group [–COO^-] of the capping agent (citric acid) in the reaction solution; as the pH is increased, the [–COO^-] increases and gives excessive capping actions. The $I_{(200)}/I_{(020)}$ and $I_{(002)}/I_{(200)}$ of nanorod films, obtained by SSL assisted by a hydrothermal reaction at different pH values, showed a slight increase of the crystal facet orientations to the WO_3 nanoplate powder sample as shown in Table 1.

For investigating the effect of various capping agents, oxalic acid was used as a capping agent in SSL assisted by a hydrothermal reaction. The micro-sized WO_3 plate film with a thickness of *ca.* 2 μm was obtained as shown in Fig. 4(a) and (b). The corresponding XRD pattern as shown in Fig. 4(c) indicates that the as-obtained plate films are composed of two kinds of crystal phases: primary monoclinic WO_3 and minor orthorhombic $WO_3 \cdot 0.33H_2O$ (JCPDS no. 72-0199). This film, also regarded as monoclinic WO_3 as explained in Fig. S3,† exhibits a similar phenomenon that the intensity of the (002) facet reflection peak is the biggest; $I_{(002)}/I_{(020)}$ is 9.60 and $I_{(002)}/I_{(200)}$ is 5.38 as shown in Table 1. It indicates that the microplates preferably grow along the same (001) direction. After ignoring the FTO peaks, orthorhombic phase peaks and most exposed (002), (020) and (200) peaks, there are still some little peaks in the pattern which means the microplate film has some irregular plate particles not vertically growing on the substrate.[28,29] In contrast, all the peaks except the (002) peak as shown in Fig. 2(c) almost disappeared which indicates that the nanorod film is more regular and perpendicular to the FTO substrate. Although only a few groups have synthesized tungsten trioxide nanorod films on FTO substrates,[24,30–32] the XRD patterns of their films actually show many high intensity peaks. To the best of our knowledge, this is

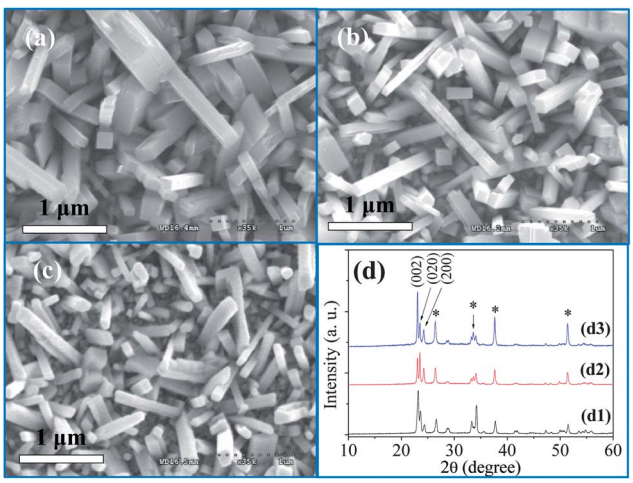

Fig. 3 SEM images and XRD patterns of WO_3 films synthesized by the spin-coating seed layer assisted by a hydrothermal method at 180 °C for 12 h using 0.1 mol citric acid as a capping agent at different pH values. (a and d1) Initial pH 1.9, (b and d2) pH 2.3, and (c and d3) pH 2.5 (Low magnification images are shown in Fig. S2†).

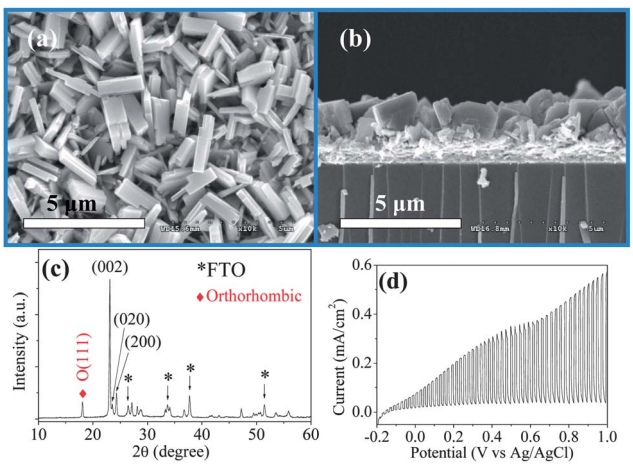

Fig. 4 (a) Top-view and (b) cross-sectional SEM images and (c) XRD pattern of the WO_3 film synthesized by the spin-coating seed layer assisted by a hydrothermal method at 180 °C for 24 h using 0.1 mol oxalic acid as the capping agent. (d) Photocurrent of the film after calcination in air at 500 °C for 2 h.

the first time that the vertical growth of tungsten trioxide nanorod films has been proven using XRD patterns. The HRTEM image of WO_3 micro-sized plates after calcination in air at 500 °C for 2 h is shown in Fig. S4(a).† The clear lattice structure and SAED pattern show that the plates are single crystalline. Their crystal lattice distances of *ca.* 0.38 nm and *ca.* 0.36 nm correspond to the *d*-spacing of the (002) and (200) planes, respectively. Fig. S4(b)† shows 10 CV scanning curves of the WO_3 microplate film without calcination treatment. The curves are smooth and show nearly no obvious change after 10 cycles of scanning. This indicates that the as-obtained monoclinic WO_3 film is very stable.[10,11] The general photoelectrochemical property of the WO_3 microplate film electrode was checked under chopped (1 Hz) 1 sun light. The photocurrent onset potential of the microplate film is around −0.2 V *vs.* Ag/AgCl, which is more negative than that of the nanorod film. The photocurrent is *ca.* 0.57 mA cm^{-2} at 1.0 V *vs.* Ag/AgCl.

In this work, the high crystalline thermally stable monoclinic WO_3 films with nanorod and microplate morphologies have been synthesized by using different capping agents. The nanorod film growing on the rubbing nanoplate seed layer with high crystallinity shows high orientation along the (001) growth direction. Citric acid can be used as a capping agent for nanorod growth and the morphologies of products are sensitive to the pHs of reaction solution. The microplate film directly growing on the normal spin-coating seed layer is also (001) oriented. According to this work, it is possible to make perfectly (001)-oriented WO_3 films if the perfect rubbing seed layer can be made.

This work was supported by the Korea Center for Artificial Photosynthesis (KCAP) located in Sogang University funded by the Ministry of Education, Science, and Technology (MEST) through the National Research Foundation of Korea (no. 2012M1A2A2671783).

Notes and references

1 A. Kudo and Y. Miseki, *Chem. Soc. Rev.*, 2009, **38**, 253.
2 J. E. Yourey and B. M. Bartlett, *J. Mater. Chem.*, 2011, **21**, 7651.
3 X. Liu, F. Wang and Q. Wang, *Phys. Chem. Chem. Phys.*, 2012, **14**, 7894.
4 F. G. Wang, C. D. Valentin and G. Pacchioni, *J. Phys. Chem. C*, 2012, **116**, 10672.
5 R. Chatten, A. V. Chadwick, A. Rougier and P. J. D. Lindan, *J. Phys. Chem. B*, 2005, **109**, 3146.
6 M. Li, E. I. Altman, A. Posadas and C. H. Ahn, *Surf. Sci.*, 2003, **542**, 22.
7 Á. Valdés and G.-J. Kroes, *J. Chem. Phys.*, 2009, **130**, 114701.
8 H. Jin, J. Zhu, J. Hu, Y. Li, Y. Zhang, X. Huang, K. Ding and W. Chen, *Theor. Chem. Acc.*, 2011, **130**, 103.
9 Y. P. Xie, G. Liu, L. Yin and H. M. Chen, *J. Mater. Chem.*, 2012, **22**, 6746.
10 Z. Jiao, X. W. Sun, J. Wang, L. Ke and H. V. Demir, *J. Phys. D: Appl. Phys.*, 2010, **43**, 285501.
11 Z. Jiao, J. Wang, L. Ke, X. Liu, H. V. Demir, M. F. Yang and X. W. Sun, *Electrochim. Acta*, 2012, **63**, 153.
12 Z. Jiao, X. Wang, J. Wang, L. Ke, H. V. Demir, T. W. Koh and X. W. Sun, *Chem. Commun.*, 2012, **48**, 365.
13 L. J. LeGore, K. Snow, J. D. Galipeau and J. F. Vetelino, *Sens. Actuators, B*, 1996, **35**, 164.
14 M. D. Giulio, D. Manno, G. Micocci, A. Serra and A. Tepore, *J. Phys. D: Appl. Phys.*, 1997, **30**, 3211.
15 Z. Jiao, J. Wang, L. Ke, X. W. Sun and H. V. Demir, *ACS Appl. Mater. Interfaces*, 2011, **3**, 229.
16 J. C. Hill and K. S. Choi, *J. Phys. Chem. C*, 2012, **116**, 7612.
17 Y. Kobayashi, S. Terada and K. Kubota, *Thin Solid Films*, 1989, **168**, 133.
18 L. J. LeGore, O. D. Greenwood, J. W. Paulus, D. J. Frankel and R. J. Lad, *J. Vac. Sci. Technol., A*, 1997, **15**, 1223.
19 A. Garg, J. A. Leake and Z. H. Barber, *J. Phys. D: Appl. Phys.*, 2000, **33**, 1048.
20 P. Tagtstrom and U. Jansson, *Thin Solid Films*, 1999, **352**, 107.
21 M. J. Wang, G. J. Fang, L. Y. Yuan, H. H. Huang, Z. H. Sun, N. S. Liu, S. H. Xia and X. Z. Zhao, *Nanotechnology*, 2009, **20**, 185304.
22 S. Ling, D. Mei and M. Gutowski, *Catal. Today*, 2011, **165**, 41.
23 C. Santato, M. Odziemkowski, M. Ulmann and J. Augustynski, *J. Am. Chem. Soc.*, 2001, **123**, 10639.
24 J. Su, X. Feng, J. D. Sloppy, L. Guo and C. A. Grimes, *Nano Lett.*, 2011, **11**, 203.
25 T. Kawashima, H. Matsui and N. Tanabe, *Thin Solid Films*, 2003, **445**, 241.
26 J. S. Lee, J. H. Kim, Y. J. Lee, N. C. Jeong and K. B. Yoon, *Angew. Chem., Int. Ed.*, 2007, **46**, 3087.
27 J. Zhu, S. Wang, S. Xie and H. Li, *Chem. Commun.*, 2011, **47**, 4403.
28 H. Ishihara, G. K. Kannarpady, K. R. Khedir, J. Woo, S. Trigwell and A. S. Biris, *Phys. Chem. Chem. Phys.*, 2011, **13**, 19553.
29 X. Q. An, J. C. Yu, Y. Wang, Y. M. Hu, X. L. Yu and G. J. Zhang, *J. Mater. Chem.*, 2012, **22**, 8525.
30 J. Su, L. Guo, N. Bao and C. A. Grimes, *Nano Lett.*, 2011, **11**, 1928.
31 W. Smith, A. Wolcott, R. C. Fitzmorris, J. Z. Zhang and Y. Zhao, *J. Mater. Chem.*, 2011, **21**, 10792.
32 S. S. Kalanur, Y. J. Hwang, S. Y. Chae and O. S. Joo, *J. Mater. Chem. A*, 2013, **1**, 3479.

